

Star-forming Main Sequence of Giant Low Surface Brightness Galaxies

WEI DU,¹ CHENG CHENG,^{2,3} PENGLIANG DU,^{3,4} LIN DU,^{3,4} AND HONG WU³

¹Key Laboratory of Optical Astronomy, National Astronomical Observatories, Chinese Academy of Sciences, Beijing, 100101, China; wdu@nao.cas.cn

²Chinese Academy of Sciences South America Center for Astronomy, National Astronomical Observatories, CAS, Beijing 100101, China

³Key Laboratory of Optical Astronomy, National Astronomical Observatories, Chinese Academy of Sciences, Beijing, 100101, China

⁴School of Astronomy and Space Science, University of Chinese Academy of Sciences, 19A Yuquan Road, Shijingshan District, Beijing, 100049, China

ABSTRACT

Giant Low Surface Brightness Galaxies (GLSBGs) are fundamentally distinct from normal galaxies and other types of low surface brightness galaxies (LSBGs) in star formation and evolution. In this work, we collected 27 local GLSBGs from the literature. They have high stellar masses ($M_* > 10^{10} M_\odot$) and low FUV-based star formation rates (SFRs). With the specific SFRs (sSFR) lower than the characteristic value of the local star-forming galaxies of $M_* = 10^{10} M_\odot$ ($\text{sSFR} < 0.1 \text{ Gyr}^{-1}$), GLSBGs deviate from the star formation main sequence (MS) defined for local star-forming galaxies respectively by Elbaz et al. (2007) (E07) and Saintonge et al. (2016) (S16) at the high M_* regime. They are HI-rich systems with the HI gas mass fractions (f_{HI}) higher than the S16 MS galaxies, but have little molecular gas (H_2), implying a quite low efficiency of HI-to- H_2 transition due to the low HI surface densities (Σ_{HI}) that are far lower than the minimum Σ_{HI} of $6 - 8 M_\odot \text{ pc}^{-2}$ required for shielding the formed H_2 from photodissociation. For GLSBGs, the inner, bulge-dominated part with lower SFRs and higher M_* is the main force pulling the entire GLSBG off from the MS, while the outer, disk-dominated part with relatively higher SFRs and lower M_* reduces the deviations from the MS. For some cases, the outer, disk-dominated parts even tend to follow the MS. In the aspect of NUV - r versus $g - r$ colors, the outer, disk-dominated parts are blue and behave similarly to the normal star-forming galaxies while the inner, bulge-dominated parts are in statistics red, indicating an inside-out star formation mechanism for the GLSBGs. They show few signs of external interactions in morphology, excluding the recent major merger scenario.

Keywords: low surface brightness galaxies — star formation rate — stellar mass — star formation mechanism — HI — H_2 — gas surface density

1. INTRODUCTION

The star formation and evolution of galaxies are regulated by various environmental-dependent processes, such as mergers and interactions (Toomre 1977) that could trigger the violent star formation activity, and strangulation or starvation (Larson et al. 1980), ram pressure stripping (Gunn & Gott 1972), and galaxy harassment (Moore et al. 1996) that could quench the star formation of galaxies. Different processes shape galaxies to follow some physical scaling relations, which retain the imprint of galaxy formation and evolution. Among those scaling relations, an important one is the relation between star formation rate (SFR) and stellar mass (M_*) for star-forming galaxies, dubbed as star formation main sequence (MS; Brinchmann et al. (2004); Daddi et al. (2007); Elbaz et al. (2007); Noeske et al. (2007a,b); Wuyts et al. (2011)). The MS tells that star-forming galaxies populate a narrow sequence in SFR - M_* plane with a small intrinsic scatter of ~ 0.3 dex (Noeske et al. 2007a,b), which places strong constraints on the regulation of star formation processes of galaxies. The MS was originally defined for local star-forming galaxies, and later verified to be still present in higher redshifts but migrated dramatically to higher SFRs in higher redshift regimes. It implies that star-forming galaxies form their stars at a roughly steady state associated with stellar mass during most of their lifetime, and deviations in star formation are short-lived until the galaxy is finally quenched and drops off from the

MS (Cooke et al. 2023). However, starburst galaxies are featured by intense star formation in a short period, so they are high above the MS shape. Passive galaxies with low star formation fall off the MS shape.

Low Surface Brightness Galaxies (LSBGs) are traditionally defined as those galaxies with central surface brightness ($\mu_{0,B}$) at least one magnitude fainter than the night sky brightness ($\mu_{0,B} > 22.5$ mag arcsec $^{-2}$) (McGaugh 1994; de Blok et al. 1995; Impey & Bothun 1997; Bothun et al. 1997). Galaxies satisfying this definition cover a wide range of physical properties, such as size, luminosity, morphology, color, and environment. They cover from dwarf irregulars to giant spirals, from blue to red, and live in both fields and galaxy clusters. In contrast to galaxies with normal(high) surface brightnesses, the LSB disks tend to be poor in metal(McGaugh 1994) and dust, rich in neutral hydrogen gas (HI) but have low star formation rates. They are a heterogeneous collection of galaxies from diverse origins, and the mechanisms of star formation and evolution of different LSBG populations are still in question. In order to explore the star formation of dwarf LSBGs, McGaugh et al. (2017) studied a sample of dwarf LSBGs in the SFR - M_* plane, proposing that dwarf LSBGs are an entirely different population deviating from the MS galaxies. Differing from dwarf LSBGs, giant LSBGs (GLSBGs; Bothun et al. (1987); Impey & Bothun (1989); Bothun et al. (1990); Sprayberry et al. (1993)) have extremely large, diffuse disks. They are very rare in the local universe ($z < 0.1$) and represent the large-size end of the number density distribution of normal-size spiral galaxies (Saburova et al. 2023). GLSBGs have fundamentally different origins, star formation histories and evolutionary paths from dwarf and other LSBGs. So far, few studies have been dedicated to the investigation of a sample of GLSBGs in the MS plane. In this work, we would study the GLSBGs in the MS plane in order to explore the underpinning star formation processes of GLSBGs.

We collect GLSBGs and describe the multi-wavelength imaging data in Section 2.1, and estimate the star formation rates (SFRs) and stellar masses (M_*) in Section 2.2. We study GLSBGs in the SFR - M_* plane in Section 3.1, HI gas in Section 3.2 and constrain H_2 gas in Section 3.3. The inner and outer parts of each GLSBG are separately studied in the SFR - M_* plane, and the formation mechanism is discussed in Section 4. In Section 5, the whole work is summarised. All the distance-dependent quantities in this work are computed assuming a Λ CDM cosmology with $H_0 = 70$ km s $^{-1}$ Mpc $^{-1}$, $\Omega_m = 0.3$ and $\Omega_\Lambda = 0.7$. The Chabrier (2003) initial mass function (Chabrier IMF) is assumed and AB magnitudes are used throughout the paper.

2. DATA

2.1. Sample

It is estimated that there are around 12,700 GLSBGs in the entire sky out to $z < 0.1$ (Saburova et al. 2023), but only a handful of them (less than 100) have been truly observed and identified in the literature so far (Kent 1985; Sprayberry et al. 1993; McGaugh & Bothun 1994; Sprayberry et al. 1995; McGaugh et al. 1995; Pickering et al. 1997; Schombert 1998; Matthews et al. 2001; Rahman et al. 2007; Mishra et al. 2015; Galaz et al. 2015; Hagen et al. 2016; Boissier et al. 2016; Mishra et al. 2017). We collected 27 designated GLSBGs (Table 1) observed by both GALEX ultraviolet (FUV, NUV) (Morrissey et al. 2007; Bianchi 2014; Bianchi et al. 2014) and DECaLS (Dey et al. 2019) optical (g , r) imaging surveys from the literature as the sample. Seventeen galaxies of the sample (denoted as S17; the first 17 galaxies in Table 1) meet the ‘diffuseness index’ criterion $\mu_B(0) + 5 \log(R_s) > 27.0$ by Sprayberry et al. (1995) where $\mu_B(0)$ is the disk B-band central surface brightness in mag arcsec $^{-2}$ and R_s is the disk scale length in h^{-1} kpc based on a distance scale with $H_0 = 100$ km s $^{-1}$ Mpc $^{-1}$. The rest ten galaxies of the sample (denoted as S10; the last 10 galaxies in Table 1) are from Schombert (1998) that defined GLSBGs with low central surface brightness ($\mu_0(B) > 22$ mag arcsec $^{-2}$) or mean surface brightness ($\mu_{\text{eff}}(B) > 24$ mag arcsec $^{-2}$), large diameter ($D > 20$ kpc) and high HI mass ($M_{\text{HI}} > 3.1 \times 10^9 M_\odot$). Although the two selection criteria are seemingly different, they fundamentally aim to pick out galaxy populations that are large in size (stellar mass) and simultaneously have low surface brightness. However, the ‘diffuseness index’ criterion only constrains a GLSBG in size and surface brightness, lacking some constraint for the stellar mass or luminosity, so some galaxies could meet the ‘diffuseness index’ criterion by their large size and low surface brightness, but are not conventionally giant in luminosity or stellar mass, such as UGC 9024 in our sample. Although UGC 9024 is not a giant in stellar mass, it is indeed identified by the ‘diffuseness index’ criterion and studied as a GLSBG McGaugh & Bothun (1994); Sprayberry et al. (1995); McGaugh et al. (1995); Pickering et al. (1997); Matthews et al. (2001); Rahman et al. (2007). Therefore, we also include UGC 9024 in our sample, but mark it (a blue filled diamonds) in figures.

Table 1. The 27 GLSBGs collected from the literature

GLSBG	RA	DEC	velocity	MHI	err _{MHI}	ref ^a
Name	deg	deg	(km/s)	10 ¹⁰ M _⊙	10 ¹⁰ M _⊙	
(1)	(2)	(3)	(4)	(5)	(6)	(7)
0052-0119	13.7872	-1.0465	13197	-	-	3
0221+0001	36.0057	0.2523	37263	-	-	3
0237-0159	40.0461	-1.7744	12701	-	-	3
1034+0220	159.3653	2.0895	21335	-	-	3
1226+0105	187.3036	0.8178	23655	3.71	-	9,3,14
F533-3	334.3049	25.2130	12396	1.74	-	10
Malin-1	189.2473	14.3304	23793	4.57	-	6,14,7,8
Malin-2	159.9687	20.8470	13494	3.60	0.40	14,1,2
NGC4017	179.6901	27.4523	3428	1.70	0.35	12,3,14
NGC5533	214.0321	35.3437	3818	1.00	0.44	12,3,14
NGC5905	228.8472	55.5171	3350	2.45	-	12,3,14
NGC7589	349.5654	0.2612	8792	1.02	-	10,14
UGC1382	28.6711	-0.1434	5767	1.70	0.10	5
UGC1752	34.0869	24.8883	17847	1.78	-	4,10
UGC6614	174.8118	17.1436	6353	2.50	0.20	13,15,14,4,2,1
UGC9024	211.6689	22.0700	2311.0	0.25	-	13,15,3,14,10,11
UM163 ^b	352.6348	-2.4625	10022.0	0.34	0.04	2,1,3
UGC12740	355.4723	23.8150	10522	1.12	0.13	4
UGC12845	358.9245	31.8997	4880	0.58	0.25	4
UGC1455	29.6999	24.8925	5070	3.72	0.60	4
UGC1922	36.9410	28.2092	10894	3.20	0.40	1,2,4
UGC3968	115.6885	66.2584	6780	0.96	-	4
UGC4219	121.6783	39.0902	12433	2.95	-	4
UGC4422	126.9249	21.4791	4330	1.50	0.50	1,2,4
UGC4985	140.7210	21.9753	10180	3.02	0.35	4
UGC6754	176.6966	20.6754	7023.0	2.09	0.29	4
UGC905	20.4467	23.7809	11465.0	1.32	0.15	4

NOTE—

a. The ref No.s refer to the following papers. 1 - Mishra et al. (2017), 2 - Mishra et al. (2015), 3 - Sprayberry et al. (1995), 4 - Schombert (1998), 5 - Hagen et al. (2016), 6 - Bothun et al. (1987), 7 - Galaz et al. (2015), 8 - Boissier et al. (2016), 9 - Sprayberry et al. (1993), 10 - Matthews et al. (2001), 11 - Rahman et al. (2007), 12 - Kent (1985), 13 - McGaugh & Bothun (1994), 14 - Pickering et al. (1997), and 15 - McGaugh et al. (1995).

b. UM163 is also known as 2327-0244 in ref NOs. 3.

2.2. SFR and Stellar Mass

We obtain image frames of FUV, NUV (GALEX DR6), g , r , and z bands (DECaLS DR9) for each GLSBG in our sample. Then, we match the Point Spread Functions (PSFs) of the image frames of FUV, g , r , and z bands to the PSF of NUV band that is the lowest among the five bands. The surrounding bright stars of the target GLSBG are masked from the PSF-matched image frames to reduce light pollution. The reduced images of the five bands for each GLSBG

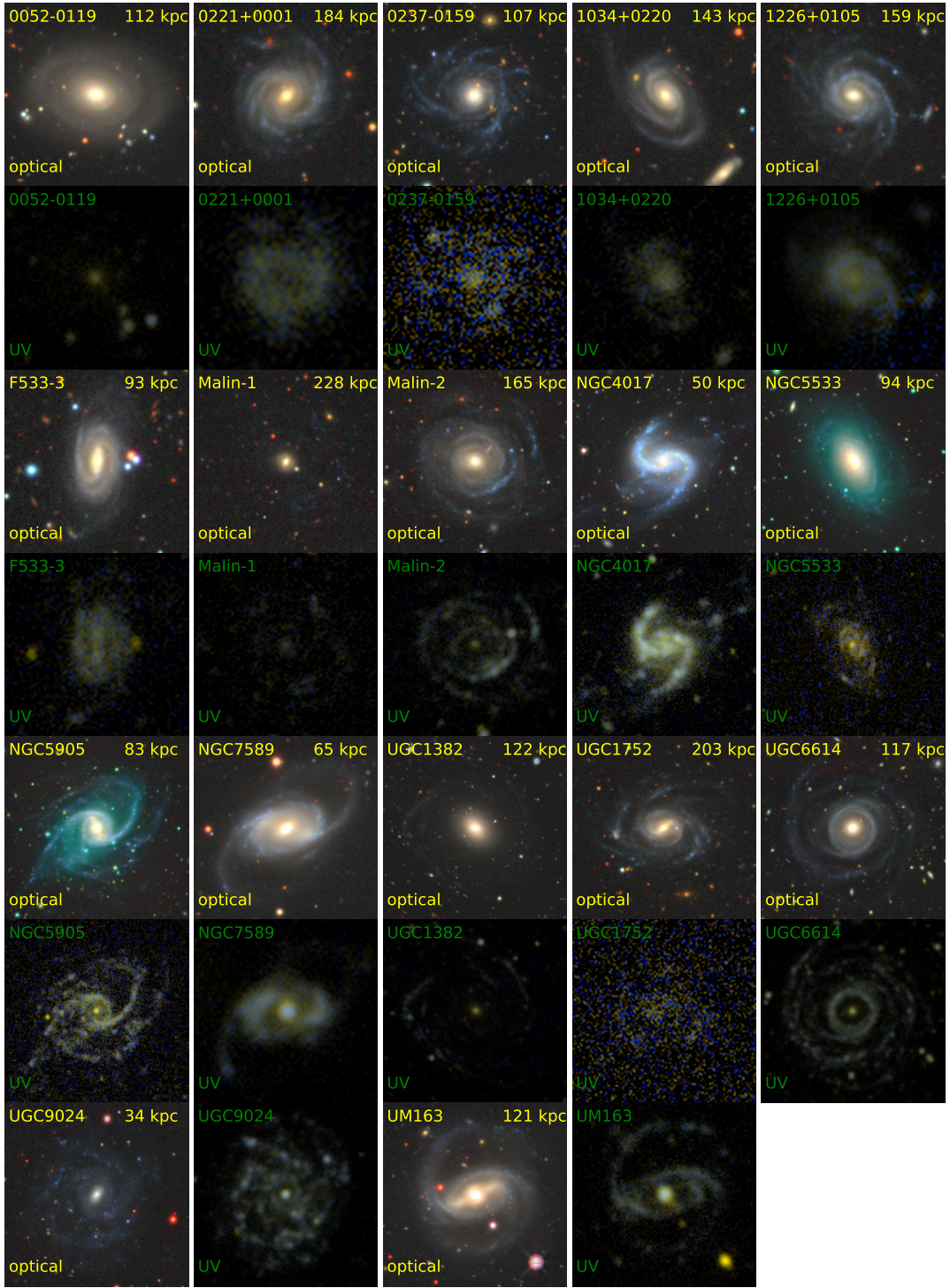


Figure 1. Images of the 17 GLSBGs definitely meeting the ‘diffuseness index’ criterion. For each galaxy, we show its optical and UV images, respectively, in individual frames of the same physical size labeled at the top right of the optical frame. The optical image is the g -, r -, and z -composite image from DECaLS, except for NGC5533 and NGC5905 which have no z -band images from DECaLS, and the UV image is the FUV- and NUV-composite image from GALEX.

Table 2. Measured properties of the 27 GLSBGs.

GLSBG	FUV	err _{FUV}	NUV	err _{NUV}	g	err _g	r	err _r	SFR ^a	err _{SFR}	M _* ^a
Name	mag	mag	mag	mag	mag	mag	mag	mag	M _⊙ /yr	M _⊙ /yr	10 ¹¹ M _⊙
(1)	(2)	(3)	(4)	(5)	(6)	(7)	(8)	(9)	(10)	(11)	(12)
0052-0119	20.690	0.102	18.826	0.042	14.467	0.003	13.676	0.002	0.06	0.010	2.02
0221+0001	18.914	1.303	18.559	0.057	16.485	0.002	15.755	0.002	2.84	3.553	3.54
0237-0159	17.653	0.701	17.323	0.033	15.287	0.002	14.663	0.002	0.94	0.653	0.89
1034+0220	19.509	0.056	18.738	0.660	15.868	0.001	15.129	0.001	0.50	0.053	1.48
1226+0105	18.412	0.968	18.046	0.047	15.731	0.002	15.087	0.002	1.57	1.479	1.40
F533-3	18.162	1.001	17.758	0.041	14.961	0.011	14.248	0.007	0.56	0.544	1.35
Malin-1	19.515	0.063	18.912	0.702	16.764	0.016	15.994	0.011	0.63	0.070	0.97
Malin-2	17.402	0.614	17.062	0.020	14.285	0.004	13.582	0.002	1.34	0.824	1.98
NGC4017	14.952	0.199	14.646	0.008	12.833	0.001	12.383	0.001	0.79	0.177	0.27
NGC5533	15.930	0.301	15.582	0.143	12.142	0.002	11.389	0.001	0.40	0.128	1.08
NGC5905	14.789	0.178	14.534	0.008	12.145	0.001	11.490	0.001	0.87	0.179	0.57
NGC7589	17.458	0.030	17.112	0.156	14.354	0.004	13.679	0.003	0.53	0.040	0.88
UGC1382	17.709	0.722	17.439	0.025	13.714	0.002	12.919	0.001	0.18	0.127	0.79
UGC1752	17.578	0.799	17.431	0.398	14.946	0.004	14.261	0.003	1.91	1.502	1.80
UGC6614	16.535	0.435	15.991	0.013	13.718	0.002	13.067	0.001	0.63	0.281	0.93
UGC9024 ^b	16.599	0.431	16.387	0.021	14.983	0.003	14.599	0.002	0.08	0.035	0.010
UM163 ^c	16.964	0.055	16.449	0.016	13.402	0.003	12.802	0.002	1.09	0.106	1.81
UGC12740	17.710	0.796	17.284	0.414	15.235	0.006	14.717	0.004	0.58	0.457	0.31
UGC12845	16.388	0.423	16.164	0.02	13.509	0.003	12.895	0.002	0.42	0.182	0.45
UGC1455	15.794	0.377	15.735	0.195	12.619	0.015	11.858	0.010	0.80	0.313	1.56
UGC1922	17.220	0.046	16.537	0.036	13.509	0.011	12.955	0.007	0.98	0.088	2.04
UGC3968	16.670	0.458	16.368	0.232	13.955	0.003	13.293	0.002	0.64	0.298	0.47
UGC4219	16.807	0.512	16.504	0.023	14.132	0.005	13.488	0.003	1.89	0.977	1.10
UGC4422	15.332	0.249	14.970	0.013	12.444	0.001	11.849	0.001	0.87	0.237	0.92
UGC4985	16.983	0.524	16.440	0.019	13.617	0.003	12.922	0.002	1.06	0.564	2.22
UGC6754	15.844	0.303	15.496	0.012	12.807	0.003	12.139	0.002	1.45	0.467	1.75
UGC905	19.138	1.585	18.445	0.618	14.788	0.005	13.997	0.004	0.19	0.282	1.17

NOTE—

- a. SFRs and M_{*} are in the Chabier IMF. SFRs are from FUV flux with no correction for dust attenuation.
- b. This galaxy is identified as a giant LSBG according to the ‘diffuseness index’ criterion in references of No.s 3, 10, 11,13, 14, and 15 in Table 1, although it does not seem to be a giant in stellar mass in this table.
- c. UM163 is also known as 2327-0244 in [Sprayberry et al. \(1995\)](#).

are simultaneously fed into the SExtractor code to measure the flux in each band. In the dual mode of SExtractor, the extraction and the Kron aperture for photometry of the target GLSBG are first defined in the reduced *r*-band image frame, and then applied in image frames of the other four bands. The measured fluxes are next converted to magnitudes. All the magnitudes are corrected for the effects of Galactic extinction via $A_\lambda = R_\lambda E(B-V)$ where R_λ is the ratio of the total absorption A_λ to the reddening $E(B-V)$ along the line of sight to an object. For each GLSBG, the $E(B-V)$ value are estimated by [Schlafly & Finkbeiner \(2011\)](#)(SF11). In the optical *g*, *r*, and *z* bands, the extinction coefficients R_λ ($\lambda = g, r, z$) are, respectively, provided in SF11 at $R_V=3.1$. In FUV and NUV bands, the extinction coefficients of $R_{FUV} = 8.29$ and $R_{NUV} = 8.87$ are assumed.

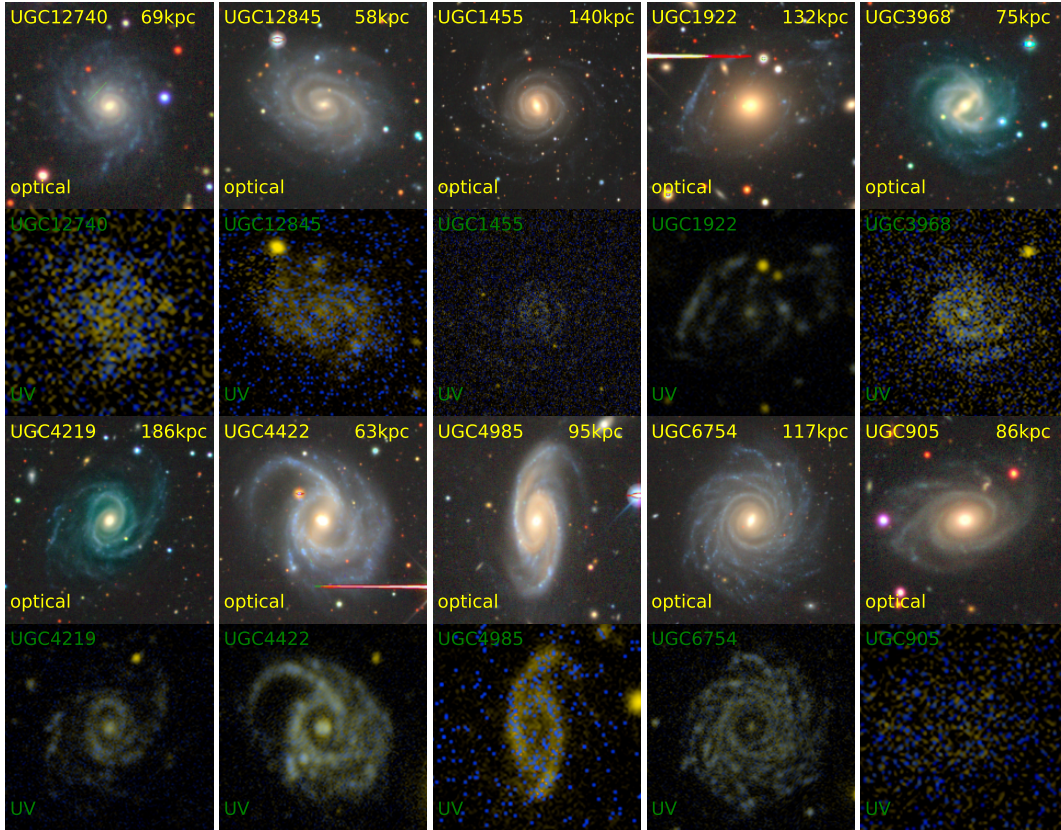


Figure 2. Images of the rest 10 GLSBGs from Schombert (1998). The illustration for this figure is the same as Figure 1. UGC3968 and UGC4219 have no z -band images from DECaLS so their optical images are the composite of only g - and r -band images from DECaLS.

Star formation rate (SFR) can be estimated from the FUV flux for each GLSBG. As the extended LSB disks are acknowledged to be deficient in dust Rahman et al. (2007), at first we do not correct the effect of internal dust extinction for FUV flux. Adopting the luminosity distance (d_L) calculated at the galaxy’s redshift (z ; corresponding to the radial velocity in Table 1) in the Λ CDM cosmology, FUV flux is converted to FUV luminosity (L_{FUV}) that is subsequently converted to SFR via the empirical relation between L_{FUV} and SFR (Salim et al. 2007). In addition, we still derive a set of dust-corrected SFRs for GLSBGs in our sample for comparison. We calculate FUV attenuation (A_{FUV}) from NUV - FUV color by using the prescription in Salim et al. (2007). Then, the dust-corrected FUV fluxes are used to estimate dust-corrected SFRs. It is worth noting that during dust attenuation correction for FUV fluxes, we find that the estimated A_{FUV} have extremely large errors (even larger than the values themselves) that further introduce very large uncertainties to the dust-corrected SFRs that have errors at least 2~3 times larger than the SFR values themselves (see the error bars in the right panel of Figure 3). Therefore, we prefer the SFRs without dust correction (Table 2; the left panel of Figure 3).

Stellar mass (M_*) of each GLSBG is derived from fitting the UV-optical SEDs by using CIGALE (Noll et al. 2009; Boquien et al. 2019). We opt to use Bruzual & Charlot (2003) (BC03) stellar population model, the Chabrier IMF, the two-component exponential star formation histories, and the modified dust attenuation laws (Boquien et al. 2019). For the parameters of the adopted two-component exponential model, the formation time of the old population spans a range from 10 Gyr to 12 Gyr before the observation epoch, with e-folding times that span a range from 500 Myr to 5 Gyr. For the young population, the formation time spans from 500 Myr to 5 Gyr with a constant e-folding time of 20 Gyr. Thus, the star formation histories adopted look like old exponentials with distinct decay times superimposed by a relatively flat burst. The derived M_* are at 2.68×10^{10} - $3.54 \times 10^{11} M_\odot$ for the sample except for the galaxy UGC 9024 which has $M_* \sim 9.92 \times 10^8 M_\odot$, two orders of magnitude lower than the average M_* of the other GLSBGs (Table

2). It is not a conventional giant in stellar mass. However, as we mentioned in Section 2.1, this galaxy is identified as a GLSBG according to the ‘diffuseness index’ criterion in several major papers.

3. RESULTS

3.1. GLSBGs in the SFR-stellar mass plane

We show the GLSBGs (blue open circles) in the SFR - M_* plane (Figure 3). The SFRs of GLSBGs in the left panel are without dust correction and those in the right panel are dust-corrected (Section 2.2).

In both panels, GLSBGs are obviously below the MS defined for the local SDSS star-forming galaxies (SFGs; $0.04 < z < 0.1$, $5 \times 10^8 < M_* < 5 \times 10^{11} M_\odot$) by Elbaz et al. (2007) (black solid + dashed line; E07 MS). We also show the MS from Saintonge et al. (2016) that fitted SFRs as a function of M_* with a third-order polynomial (red dashed curve; S16 MS) for the local SDSS SFGs ($0.01 < z < 0.05$, $10^8 < M_* < 10^{12} M_\odot$). The S16 MS traces a flattening relation at the high mass regime ($M_* > 10^{10} M_\odot$), where the S16 MS is lower than E07 MS in SFR. For example, it is 0.16, 0.59, and 1.39 dex lower in SFR than E07 MS at $M_* \sim 10^{10}$, 10^{11} , and $10^{12} M_\odot$, respectively.

In the left panel, the majority of GLSBGs are clearly below the S16 MS curve while the GLSBGs move up to straddle the S16 MS curve in the right panel due to dust extinction correction. However, as we mentioned in Section 2.2, the dust extinction correction for these GLSBGs that are supposed to be poor in dust is so uncertain that the frustrating error bars of dust-corrected SFRs stretch downward the full figure frame and even cross the lower boundary of the figure frame in the right panel. Therefore, the positions of the blue open circles in the right panel represent the upper limits of the dust-corrected GLSBGs, and the length of the black downward arrow on each blue open circle does not represent any meaningful value, but only means that the lower error bar is too long to be fully displayed in the current frame of the right panel. Due to the very large uncertainties of the dust-corrected SFRs, we prefer the conclusions deduced from the left panel (no dust correction).

The GLSBG UGC1382 measured by Hagen et al. (2016) (the grey filled triangle; UGC1382-H) is shown to compare with our measurement for UGC 1382 (the blue filled circle). It shows our measurement is consistent with the measurement by Hagen et al. (2016) within the errors. For comparison with giant galaxies with normal(high) surface brightness, we show the massive, disk-dominated galaxies from Di Teodoro et al. (2021) (cyan open squares). The normal massive galaxies are clearly on the trajectory of E07 MS, and above the S16 MS at the high mass regime. In contrast, the GLSBGs do not behave similarly to MS galaxies and the normal massive galaxies in both SFR - M_* panels because of much lower specific SFR ($sSFR = SFR/M_*$). The $sSFR$ s of the GLSBGs are below 0.1 Gyr^{-1} (grey solid line) which is the characteristic $sSFR$ value for SFGs of $M_* = 10^{10} M_\odot$ at $z = 0$, and above the constant line representing $sSFR = 0.001 \text{ Gyr}^{-1}$ (grey dashed line). Despite normal massive galaxies, we also display the HI-rich dwarf LSBGs from Du et al. (2015, 2019) (small green circles) and the dwarf LSBGs from McGaugh et al. (2017) (magenta open diamonds). The dwarf LSBGs are slightly below the star formation MS, particularly those at the low mass regime ($M_* < 10^8 M_\odot$). They have higher $sSFR$ than GLSBGs.

Previous studies have shown that distances from MS relate to molecular gas contents and star formation efficiencies (SFE) of galaxies. Galaxies above the MS (mainly the starbursting galaxies) have high $sSFR$ s because of the enhanced molecular gas mass fractions and increased SFEs, but galaxies below the MS (mainly the bulge-dominated galaxies) have low $sSFR$ s and are observed to be low in both molecular gas mass fractions and SFEs (Saintonge et al. 2011a, 2012). The GLSBGs in this work have low molecular gas content (discussed in 3.3) and SFEs, which lead to their low $sSFR$ s.

3.2. Atomic gas versus stellar mass

We collected HI masses (M_{HI}) for 23 out of these 27 GLSBGs from the literature (Sprayberry et al. 1995; Pickering et al. 1997, 1999; Schombert 1998; Hagen et al. 2016; Mishra et al. 2017). The M_{HI} values are tabulated in Table 1. These GLSBGs are all HI-rich systems with $M_{\text{HI}} > 10^{10} M_\odot$ ($0.955 - 4.57 \times 10^{10} M_\odot$) for 20 out of 23 galaxies and $M_{\text{HI}} \sim 2.5 - 5.8 \times 10^9 M_\odot$ for the rest 3 galaxies. We show these GLSBGs (blue open circles) in the $M_{\text{HI}} - M_*$ plane (Figure 4). GLSBGs are apparent to follow the trend (black solid line) defined by Parkash et al. (2018) for a sample of HI-rich galaxies, but are clearly beyond the trajectory (grey solid line) defined by Parkash et al. (2018) for M_* -selected galaxies (brown filled squares). It implies that these GLSBGs have high HI gas mass fractions ($f_{\text{HI}} = M_{\text{HI}}/M_*$). Out of the 23 GLSBGs, 21 have $f_{\text{HI}} > 0.1$. In Figure 5, these GLSBGs (blue open circles) show higher f_{HI} than the S16 MS galaxies (blue filled circles) along M_* .

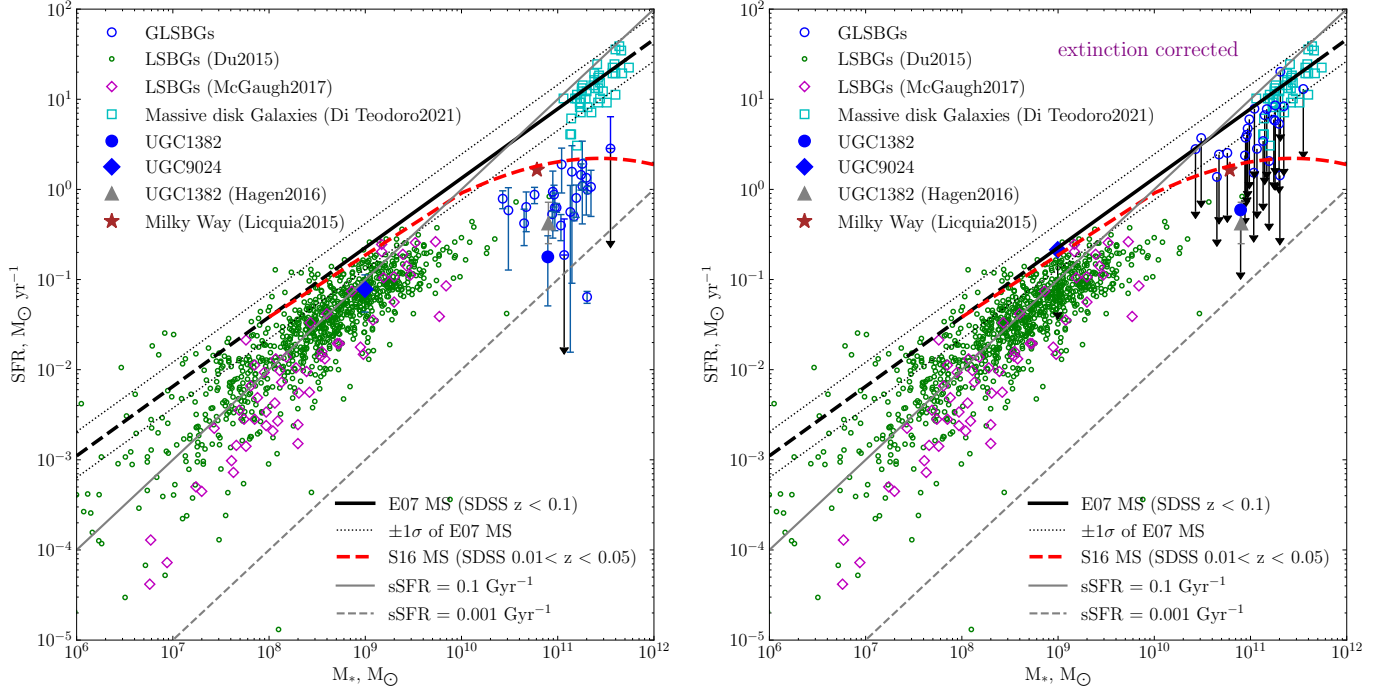


Figure 3. Star formation rate as a function of stellar mass. In both panels, GLSBGs are represented by the big blue open circles with error bars. For comparisons, the HI-rich LSBGs from Du et al. (2015) (small green circles), the dwarf LSBGs from McGaugh et al. (2017) (magenta open diamonds), massive spiral galaxies from Di Teodoro et al. (2021) (cyan open squares), the Milky Way with $M_* = 6.08 \times 10^{10} M_\odot$ and $\text{SFR} = 1.65 M_\odot \text{ yr}^{-1}$ from Licquia & Newman (2015) (red filled star), and the GLSBG UGC1382 from Hagen et al. (2016) (the grey filled triangle with error bar) are displayed as well. For a direct comparison, the UGC 1382 with our measurements in this work is highlighted by the filled blue circle. The black solid line shows the main sequence (MS) trajectory defined for the local SDSS star-forming galaxies ($0.04 < z < 0.1$, $5 \times 10^8 < M_* < 5 \times 10^{11} M_\odot$) by Elbaz et al. (2007), with the extending black, dashed lines representing its linear extrapolation to both lower mass and higher mass ends (E07 MS), and the two black dotted lines show the 68% confidence level of the E07 MS. The red dashed curve is the star formation MS trajectory defined for local SDSS galaxies ($0.01 < z < 0.05$, $10^8 < M_* < 10^{12} M_\odot$) by Saintonge et al. (2016) (S16 MS). The grey solid and dashed lines represent a constant sSFR value of 0.1 and 0.001 Gyr^{-1} . The length of the black downward arrow on some point does not refer to the actual lower error of the point, and it only means that the original lower error bar below the data point is so large that it stretches far below the figure boundary. In the left panel, SFRs are estimated from FUV flux without correction for the internal dust extinction, while in the right panel, SFRs are from dust-corrected FUV flux however, the correction is quite uncertain for this population of low surface brightness galaxies which should be very low in dust so it definitely introduces very large errors. The Chabrier IMF is assumed.

Generally, galaxies with copious amounts of HI gas should have the potential to form stars actively as HI gas is the fundamental ingredient in the formation of stars. However, GLSBGs with high HI gas fractions in this figure have very inactive star formation, indicating that the atomic hydrogen gas (HI) has not been efficiently converted into the molecular hydrogen gas (H_2) which are the direct fuel for star formation. We will discuss the low efficiency of HI -to- H_2 conversion in GLSBGs in Section 3.3.

3.3. Constraints on Molecular hydrogen gas

Molecular gas is seldom detected in the majority of GLSBGs. For instance, CO emission is never detected in Malin 1, an iconic GLSBG and also the largest spiral galaxy, even though very deep and high sensitivity observations are performed in the recent study (Galaz et al. 2022). Instead, only an upper limit (3σ) of H_2 mass ($M_{\text{H}_2} < 7.4 \times 10^9 M_\odot$) is estimated for Malin 1. Aligning the current upper limit of H_2 mass and the observed HI mass (Table 1), we could constrain the upper limit of molecular-to-atomic gas mass ratio ($R_{\text{mol}} = M_{\text{H}_2} / M_{\text{HI}}$) for Malin 1 is 0.12. However, Molecular gas is indeed detected in a few GLSBGs via CO observations (Matthews et al. 2005; Das et al. 2006, 2010). For instance, CO line emission is detected from Malin 2, a typical GLSBG, and then converted to molecular gas mass of $M_{\text{H}_2} = 4.9 - 8.3 \times 10^8 M_\odot$ through the assumed CO-to- H_2 conversion factor (Das et al. 2010). With its $M_{\text{HI}} = 3.6 \pm 0.4 \times 10^{10} M_\odot$ (Pickering et al. 1997; Das et al. 2010), Malin 2 has a molecular-to-atomic gas mass ratio (R_{mol}

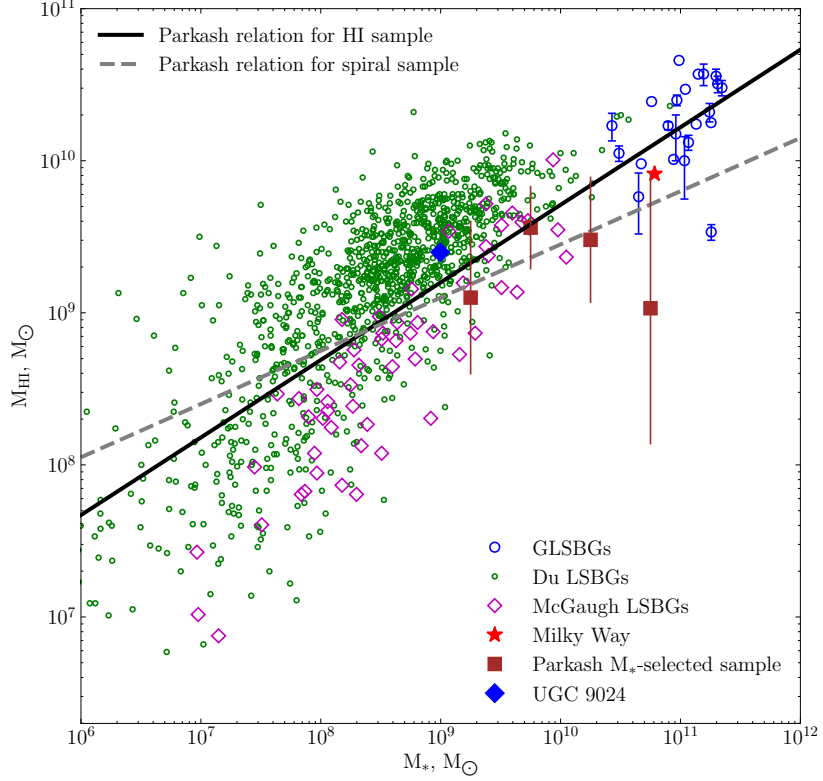


Figure 4. Relation between HI mass and stellar mass of the GLSBGs (blue open circles). For comparisons, the HI-selected LSBGs from [Du et al. \(2015\)](#) (green crosses), LSBGs from [McGaugh et al. \(2017\)](#) (magenta open diamonds), and the M_* -selected sample of galaxies binned with a width of $\log M_* = 0.5$ (brown filled squares with error bars) from [Parkash et al. \(2018\)](#), and the Milky Way (red filled star) with $M_{\text{HI}} = 8.2 \times 10^9 M_\odot$ from [Misiriotis et al. 2006](#) are displayed as well. The black solid line represents the relation followed by the HI-selected sample of galaxies with 1σ scatter of 0.5 dex, and the grey dashed line shows the relation followed by the spiral galaxies out of the M_* -selected sample with 1σ scatter of 0.4 dex from [Parkash et al. \(2018\)](#).

$= M_{\text{H}_2} / M_{\text{HI}}$) of $\sim 0.01 - 0.02$ which is relatively high for an LSB galaxy. In other few GLSBGs where CO emission is also detected, the molecular gas mass converted via the CO-to- H_2 conversion factor is in the range of $10^8 - 10^9 M_\odot$ ([Das et al. 2010](#)). As HI gas mass is typically in the level of $M_{\text{HI}} \sim 10^{10} M_\odot$ for most GLSBGs (Table 1), we can deduce the typical R_{mol} values for most GLSBGs should be $\sim 0.01 - 0.1$, which is a sufficient range to include the cases of Malin 2 ($R_{\text{mol}} \sim 0.01 - 0.1$) and Malin 1 ($R_{\text{mol}} < 0.12$). In contrast, the R_{mol} for normal massive galaxies with comparable stellar masses ($M_* \sim 10^{10} - 10^{11.5} M_\odot$) is ~ 0.3 on average [Saintonge et al. \(2011b\)](#), which is higher than GLSBGs.

According to the derived $R_{\text{mol}} \sim 0.01 - 0.1$ for GLSBGs, we calculate two sets of M_{H_2} values for GLSBGs at $R_{\text{mol}} = 0.01$ and 0.1 , respectively. The corresponding sets of H_2 gas mass fractions ($f_{\text{H}_2} = M_{\text{H}_2} / M_*$) of GLSBGs (orange open circles) are displayed in Figure 5. It is obvious that at $R_{\text{mol}} \sim 0.01 - 0.1$, GLSBGs (orange open circles) have lower f_{H_2} than S16 MS galaxies (orange filled circles) which have $R_{\text{mol}} \sim 0.3$ ([Saintonge et al. 2016](#)). This strengthens that GLSBGs are deficient in molecular gas - the direct fuel of star formation.

Given that GLSBGs are rich in HI gas (see Section 3.2) but deficient in H_2 , it is plausible that the copious amounts of HI gas has not been efficiently converted into H_2 . What causes the low efficiency of HI-to- H_2 transition? The conversion of HI-to- H_2 is closely related to metallicity, the equilibrium turbulent gas pressure, and the gas surface density ([Kasparova et al. 2014](#)). First, the low metal and dust content in GLSBGs makes the cooling of HI gas difficult and results in inefficient conversion to H_2 . Then, some research proposes that a minimum HI surface density of $\Sigma_{\text{HI}} \sim 6 - 8 M_\odot \text{pc}^{-2}$ is required to provide enough shielding for H_2 formation against photodissociation ([Lee et al. 2012](#)). Once the minimum Σ_{HI} is reached to shield H_2 from photodissociation, all excess HI is converted into H_2 and the H_2 abundance increases. However, the HI gas surface densities have been measured from the HI maps for some GLSBGs in literature, showing that the peak HI gas surface densities of these GLSBGs are indeed below the minimum value required to prevent the formed H_2 from photodissociation. For example, the peak value of Σ_{HI} is below $2 M_\odot \text{pc}^{-2}$

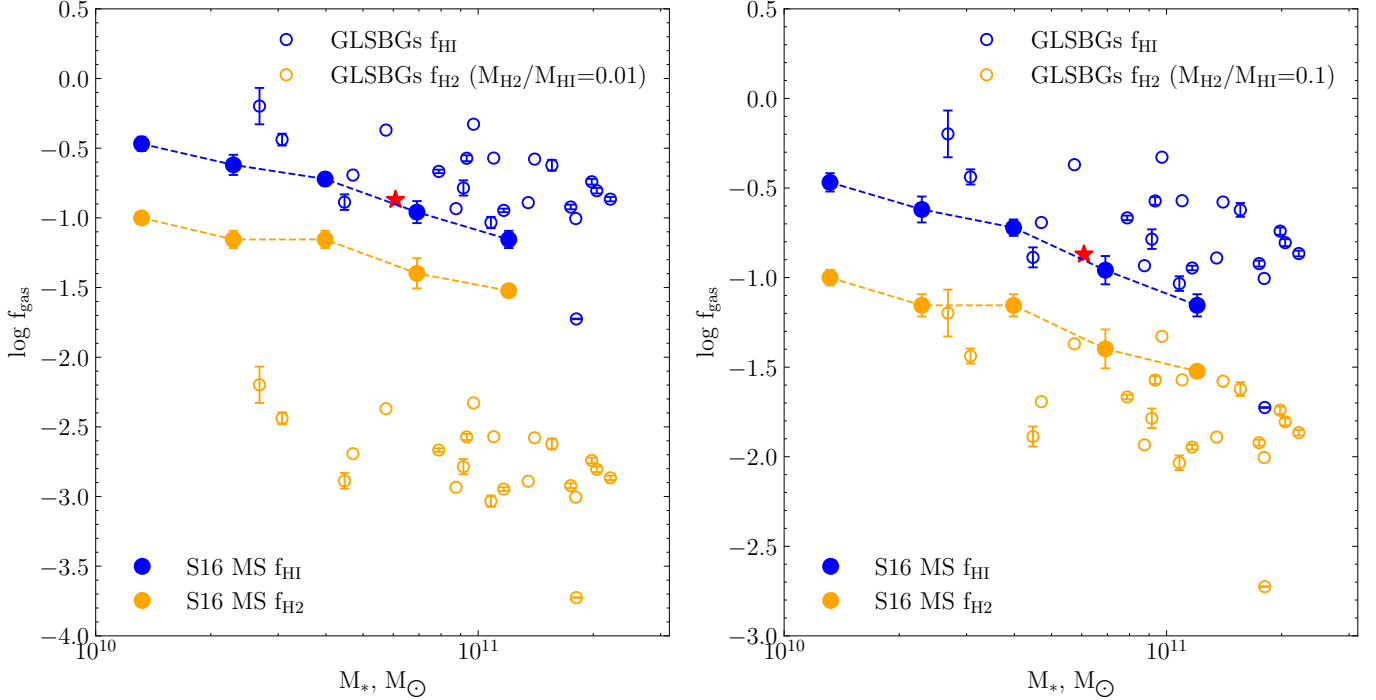


Figure 5. Gas mass fraction versus stellar mass. The open circles represent GLSBGs and the filled circles represent the mean values of five bins in M_* of S16 MS galaxies (Saintonge et al. 2016). The blue and orange colors represent HI gas mass fractions ($f_{\text{HI}} = M_{\text{HI}}/M_*$) and H₂ gas mass fractions ($f_{\text{H}_2} = M_{\text{H}_2}/M_*$). The molecular-to-atomic ratio ($R_{\text{mol}} = M_{\text{H}_2}/M_{\text{HI}}$) for GLSBGs is assumed as 0.01 in the left panel and 0.1 in the right panel. The red filled star represents the Milky Way ($M_{\text{H}_2} = 1.3 \times 10^9 M_\odot$ and $M_{\text{HI}} = 8.2 \times 10^9 M_\odot$) from Misiriotis et al. (2006).

for UGC1382 (Hagen et al. 2016), $5 M_\odot \text{ pc}^{-2}$ for Malin-1 (Lelli et al. 2010), $5.5 M_\odot \text{ pc}^{-2}$ for NGC7589 (Lelli et al. 2010), $4 M_\odot \text{ pc}^{-2}$ for UGC 6614 (Pickering et al. 1997), which are far below the minimum required HI surface density. Although we do not have HI radial surface density profiles for other individual GLSBGs yet, GLSBGs are expected to be fundamentally consistent with each other in properties, so we deduce that the lower Σ_{HI} for GLSBGs should result in low efficiency of HI- H₂ transition and thus little supply of cold gas for star formation. However, Malin 2 is an exception. As we mentioned before, Malin 2 has a relatively high fraction of molecular gas among LSBGs, and it is possibly attributed to either one or a combination of the following reasons including an underestimation of turbulent gas pressure, an incorrect CO-to-H₂ conversion factor, or a probable presence of some fraction of dark gas (invisible in CO and HI lines) which could provide additional support for the observable H₂, shielding it from being photodissociated by UV radiation Kasparova et al. (2014).

4. DISCUSSION

The star formation MS is conventionally defined based on star-forming disk galaxies, so the shape of MS should be dominantly regulated by the disks of galaxies. Recent studies proposed a turnover in MS shape at $M_* \sim 10^{10} M_\odot$, beyond which galaxies are no longer corresponding to higher SFRs due to the growth of bulge components which are quiescent and inactive in star formation activity, so they would drop off from the MS at the high mass regime. Since the disk form stars at a consistent level independent of bulge mass, the turnover should be mitigated if only the disk components are considered in high mass regime (Abramson et al. 2014; Guo et al. 2015). In terms of GLSBGs, they each host a significant bulge at the center of the extended diffuse disk (see Figure 1 and 2), so the global deviations of them from MS (Figure 3) are expected to be mainly from the bulge component. In order to validate this idea, we divide each GLSBG into inner and outer regions along the radius, and investigate the two regions separately in the SFR - M_* plane in this section.

In Section 2.2, we have measured the half-light radius ($R_{e,r}$) from the reduced (resolution-lowered to NUV and bright star-removed) r -band image for each GLSBG by using the SExtractor code. We adopt $R_{e,r}$ as a demarcation to divide each GLSBG into inner ($0 < R \leq R_e$) and outer ($R_e < R \leq R_{\text{Kron},r}$) regions on reduced FUV, NUV, g , r , and z -band

images. $R_{\text{Kron},r}$ is the Kron aperture radius for flux measurement defined by SExtractor on the reduced r -band image. For each GLSBG, we measure annular fluxes of the inner and outer regions by using *Python Aperture photometry* code, respectively, on the reduced FUV, NUV, g , r , and z -band images. Then we correct Galactic extinction for annular fluxes in each band, calculate the inner and outer SFRs from annular FUV fluxes of the inner and outer regions. For estimating the M_* of the inner and outer regions of each GLSBG, we adopt the same method of SED-fitting as described in Section 2.2. In terms of star formation history, for the inner region, we adopt a one-component exponential model of old population that has a formation time of 10 Gyr with the e-folding time spanning from 500 Myr to 5 Gyr. For the outer region, we adopt a one-component exponential model of young population that has a formation time spanning from 5 to 6 Gyr with the e-folding time from 800 Myr to 2 Gyr.

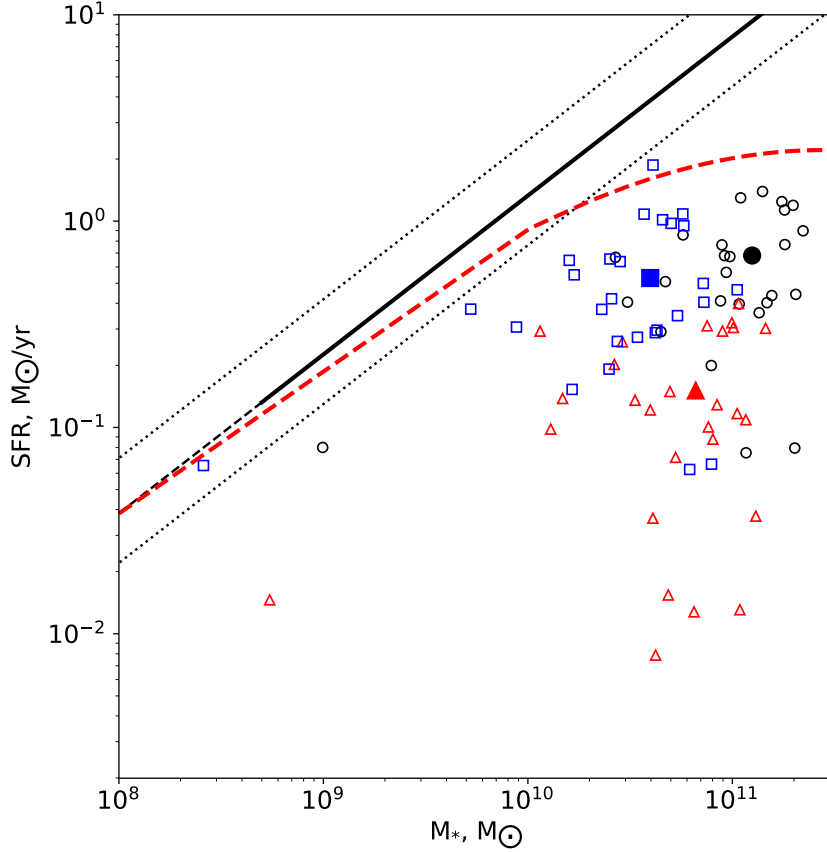


Figure 6. Star formation rate (SFR) against stellar mass (M_*) for the inner and outer regions of the 27 GLSBGs. For each galaxy, the inner, the outer, and the entire galaxy are shown as an open red triangle, an open blue square, and an open black circle. The filled red triangle, blue square, and black circle, respectively, represent the mean values for the inner, outer, and entire galaxies. The black solid line represents the E07 MS (Elbaz et al. 2007). The red dashed curve represents the S16 MS (Saintonge et al. 2016). The Chabier IMF is assumed. Note that the three isolating markers in the bottom left region in this figure are the inner, outer, and entire of UGC 9024, which is not a traditional giant galaxy in terms of stellar mass, but is identified as a GLSBG by the ‘diffuseness index’ criterion from Sprayberry et al. (1995).

We show the FUV-based SFRs against the derived M_* of the inner (open red triangles), outer regions (open blue squares), and the entire galaxies (open black circles) for the 27 GLSBGs in Figure 6, where the outer regions are systematically much closer to the MS than the outer regions which severely deviate from the MS. This tendency is more clearly revealed by the mean values of the inner (the filled red triangle), outer (the filled blue square) regions, and the entire galaxies (the filled black circle). It implies that the bulge-dominated components dominate the deviation of the entire GLSBGs from the MS due to the much lower SFRs of the bulges. However, the disk-dominated components are

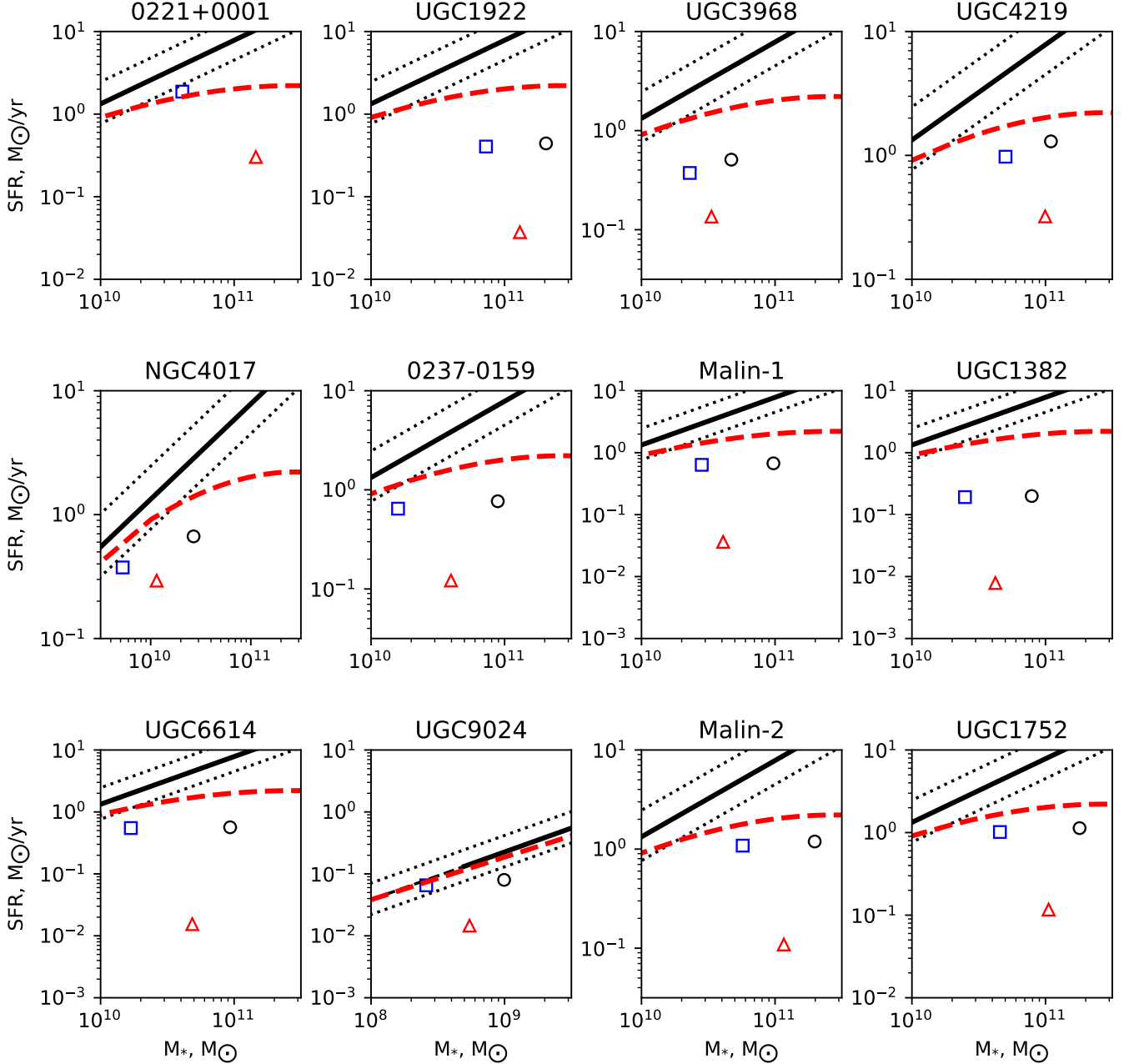


Figure 7. Star formation rate (SFR) against stellar mass (M_*) for the inner (red triangle) and outer (blue square) parts of each GLSBG. The black circle represents the entire GLSBG. The black solid line represents the E07 MS (Elbaz et al. 2007). The red dashed curve represents the S16 MS (Saintonge et al. 2016). The Chabier IMF is assumed.

the dominant contributors to the global SFR of the entire GLSBGs. If only the disk-dominated components of these GLSBGs were adopted, the deviation from the MS would be largely mitigated, with some GLSBGs even approaching to follow the MS.

Furthermore, we zoom in on each individual GLSBG in Figures 7 and 8. In both figures, the inner part (red triangle) drops off from MS (E07 - black solid line; S16 - red dashed line) more obviously, while this drop is reduced in different degrees by the outer part (blue square) for each GLSBG. The inner part of the giant galaxy is conventionally dominated by the bulge component which has little contribution to star formation but occupies a considerable contribution to the

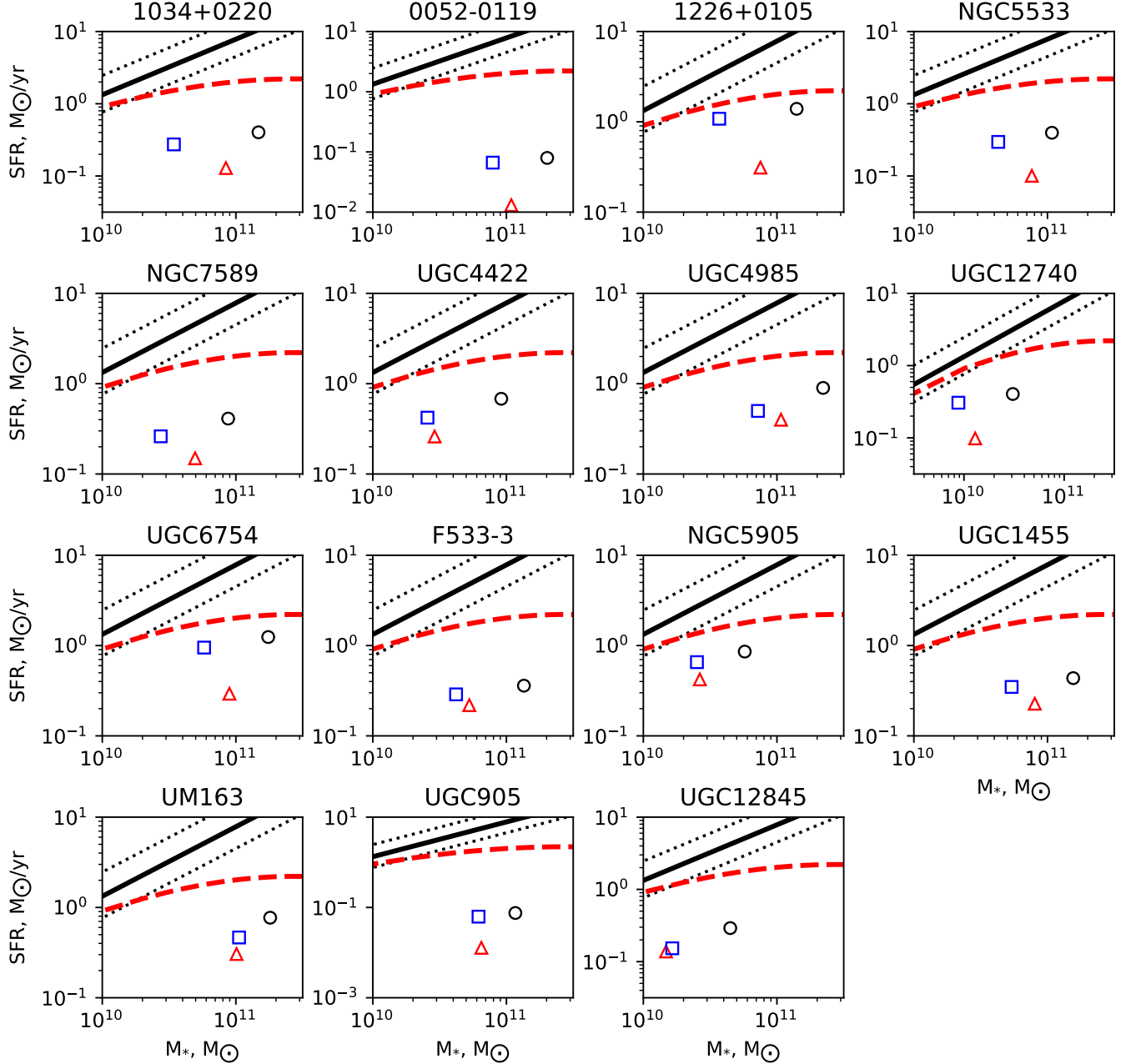


Figure 8. Continued to Figure 7.

stellar mass of the galaxy so the bulge should be the main driving force pulling the entire GLSBG off below the MS. In contrast, the outer part of the GLSBG is less affected by the central bulge component. Instead, it is mainly occupied by its large disk with relatively higher star formation but lower stellar mass than the bulge. So the deviation of the outer part from MS is reduced due to its enhanced star formation rate and decreased stellar mass. In some cases, the outer part even tends to follow the MS.

As is described in Section 2.2, in order to make sure the measured fluxes on images of different bands are from the same region of a galaxy, optical images from DECaLS g and r bands are both lowered down in resolution to match the resolution of the GALEX UV image which is much lower. However, lowering the resolution flattens the optical surface

brightness profile of the galaxy which spreads the effect of the central bulge out to the disk more, and makes it more difficult to completely decompose the bulge from the disk. We simply use $R = R_e$ as the demarcation line to divide a GLSBG into the inner and outer parts, only in order to make sure the inner part is absolutely occupied by the central bulge and the outer part is dominated by the disk in a large extent. It is evident in Figure 9, the inner parts are indeed redder than the outer parts in general under this demarcation schema. We show the boundaries of blue clouds (blue dashed), red sequence (red dashed) identified for SDSS normal galaxies Chilingarian & Zolotukhin (2012), and also the given relation between NUV - r and g - r colors defined on SDSS normal galaxies with $-23 < M_r < -21$ (black solid curve). Obviously, the outer parts (blue open squares) of GLSBGs behave similarly to the normal star-forming galaxies in the NUV - r and g - r relation (black solid curve). The inner parts of GLSBGs appear to offset above from the relation, and the inner parts of some galaxies (UGC1752, UGC1455, Malin 1, UGC1922 with the offset from small to large) are even outside the upper boundary of the red sequence identified for normal SDSS galaxies. As is investigated in Schombert (1998)(S98), the majority of GLSBGs have a sizable bulge each that is outside the morphological class, including the four inner-part outliers (UGC1752, UGC1455, Malin 1, UGC1922) in our Figure 9. This is likely a reason for the behavior of the inner parts of GLSBGs not following the relation between NUV - r and g - r at the redder end defined for normal galaxies. Besides, it is also investigated that half of the sample of GLSBGs in S98 have very low-ionization AGN behaviors, including UGC4422, UGC1455, UGC1922, UGC4219, and UGC6614 in our Figure 9. Low-ionization AGNs should have low contribution to the optical light of the inner parts of the GLSBG hosts, so this might be also a reason for the behaviors of the inner parts of GLSBGs in the figure.

As far as we can see from Figure 7 and 8, such a demarcation schema work for most of the GLSBGs since the inner and outer parts could be clearly disentangled in the aspect of SFR and M_* , although the outer M_* are not strikingly decomposed from the inner M_* as expected due to the effect of the ‘flattened’ bulge in the optical images (after the optical resolution is lowered down) on the outer part. For UM163 and UGC905, the demarcation schema does not work well as the outer M_* surpasses the inner M_* which implies that a larger radius threshold is required to better distinguish the disk-dominated part from the bulge-dominated part in the aspect of stellar mass. Albeit, in the aspect of SFR, the inner and outer parts could be distinguished in varying degrees for all GLSBGs, sufficiently demonstrating that the deviation of entire GLSBGs from the MS shape should be largely caused by the bulge components, and if only considering the pure diffuse disk, the deviation from the MS would be seriously reduced in the SFR- M_* plane. This conclusion deduced from GLSBGs well supports that the turndown of the MS shape at high M_* is mainly attributed by the growth of the central bulge that is quiescent with little SF but the disk component still tends to form stars at a consistent level with MS galaxies.

For GLSBGs, the outer parts are highly distinguished from the inner parts in NUV - r and g - r colors (Figure 9). The inner parts are quite red while the outer parts are blue, indicating divergent origins of the two parts of GLSBGs. The stellar populations of the inner parts are relatively old and must have already formed and evolved, while the stellar populations of the outer parts are relatively young and star formation is still ongoing in the outer parts. This demonstrates an inside-out star formation mechanism for GLSBGs. Additionally, these GLSBGs show few morphological signs of merging and interactions with other galaxies (Figure 1 and 2), which inclines us towards a picture that the large, extended low surface brightness disks of GLSBGs form and grow internally by themselves with little external effects after the central, bright bulge formed and evolved earlier. We plan to carry out detailed studies on the formation and evolution of GLSBGs with high resolution HI data and optical long-slit spectra in our future work.

5. SUMMARY

A sample of local GLSBGs observed by both DECaLS optical and GALEX UV imaging surveys is collected from the literature. The measurement of their stellar masses and FUV-based SFRs show that these GLSBGs have low SFRs and high M_* , deviating from the MS trajectory apparently at the high mass regime ($M_* > 10^{10} M_\odot$) in the SFR- M_* plane. Their sSFRs are lower than the characteristic value for the star-forming galaxies with $M_* = 10^{11} M_\odot$ at $z = 0$ (sSFR $< 0.1 \text{ Gyr}^{-1}$). The deviation of the GLSBG as a whole from the MS should relate to the low molecular gas content and low SFE. These GLSBGs are HI-rich systems with higher HI gas mass fractions (f_{HI}) than the S16 MS galaxies, but poor in H_2 because of quite a low efficiency of HI-to- H_2 conversion. The possible reasons for the low transition are the lack of metal and dust, and the low HI gas surface densities that are far below the minimum HI surface density of 6 - 8 $M_\odot \text{ pc}^{-2}$ required for shielding H_2 against photodissociation.

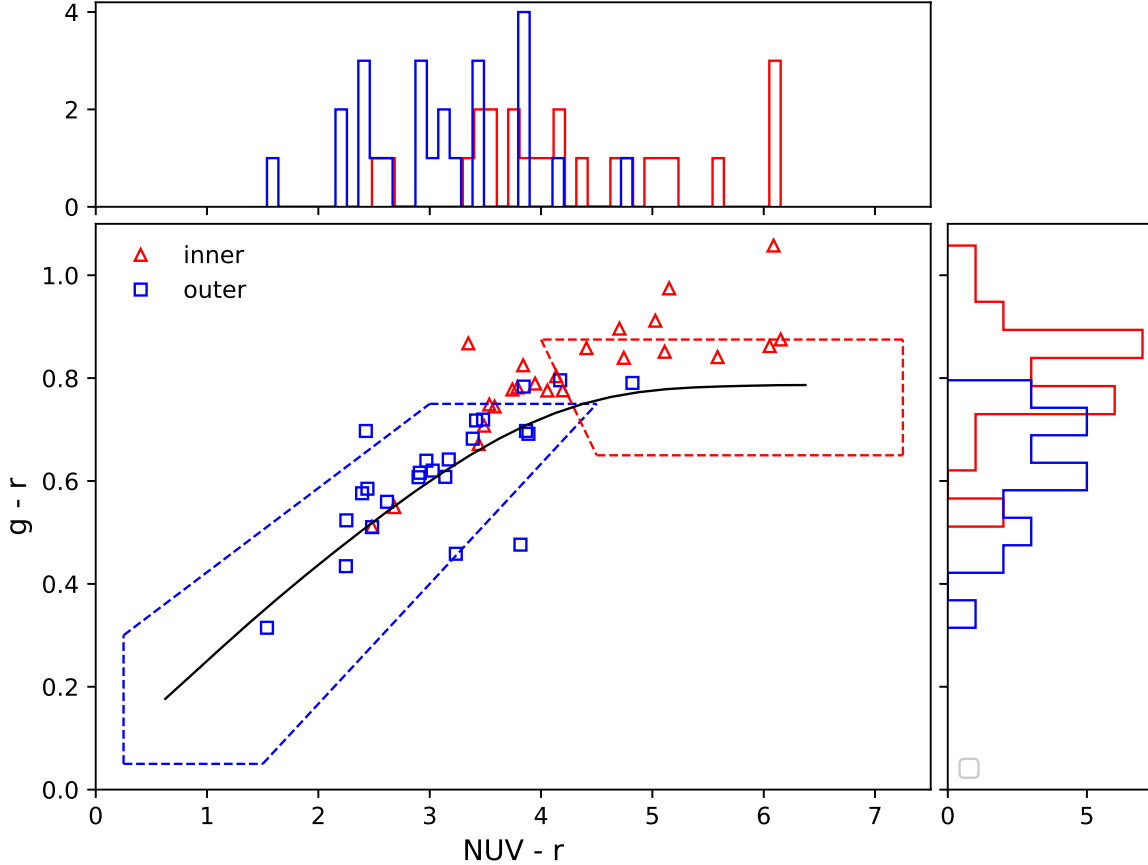


Figure 9. The colors of $NUV - r$ and $g - r$ of the inner (red triangle) and outer parts (blue square) for each GLSBG. From Chilingarian & Zolotukhin (2012), it identifies the loci of blue cloud (blue dashed) and the red sequence (red dashed) based on SDSS galaxies, and also defines the relation between $NUV - r$ and $g - r$ for SDSS galaxies with r -band absolute magnitudes $-23 < M_r < -21$ mag (black solid curve). The right and top bars show the $NUV - r$ and $g - r$ histogram distributions of the inner (red) and outer part (blue) of GLSBGs.

We discuss the contributions of the inner (bulge-dominated) and outer (disk-dominated) parts of GLSBGs to the entire deviations of GLSBGs from the MS. Generally, the bulge-dominated parts have lower SFRs and relatively higher M_* than the disk-dominated parts of GLSBGs, and are the main force pulling the entire GLSBG off from the MS. However, the deviations from the MS are clearly reduced if the disk-dominated parts of the GLSBG are only considered in the SFR - M_* plane. For some cases, the disk-dominated parts even tend to follow the MS shape. In contrast to the red, inner, bulge-dominated parts, the outer, disk-dominated parts of GLSBGs are bluer and follow the $NUV - r$ versus $g - r$ relation for normal SFGs. The color difference between the inner and outer parts also implies an inside-out mechanism for the star formation of GLSBGs. They show few signs of tidal interactions, supporting that the large, extended low surface brightness disks are not likely to grow via recent major mergers.

We thank the referee for the helpful comments. D.W. is supported by the National Natural Science Foundation of China (NSFC) grant Nos. U1931109 and the Youth Innovation Promotion Association, CAS (No. 2020057). C.C. is supported by the NSFC No. 11803044, 11933003, 12173045 and also supported by the CAS South America Center for Astronomy (CASSACA).

REFERENCES

- Abramson, L. E., Kelson, D. D., Dressler, A., et al. 2014, *ApJL*, 785, L36, doi: [10.1088/2041-8205/785/2/L36](https://doi.org/10.1088/2041-8205/785/2/L36)
- Bianchi, L. 2014, *Ap&SS*, 354, 103, doi: [10.1007/s10509-014-1935-6](https://doi.org/10.1007/s10509-014-1935-6)
- Bianchi, L., Conti, A., & Shiao, B. 2014, *Advances in Space Research*, 53, 900, doi: [10.1016/j.asr.2013.07.045](https://doi.org/10.1016/j.asr.2013.07.045)
- Boissier, S., Boselli, A., Ferrarese, L., et al. 2016, *A&A*, 593, A126, doi: [10.1051/0004-6361/201629226](https://doi.org/10.1051/0004-6361/201629226)
- Boquien, M., Burgarella, D., Roehly, Y., et al. 2019, *A&A*, 622, A103, doi: [10.1051/0004-6361/201834156](https://doi.org/10.1051/0004-6361/201834156)
- Bothun, G., Impey, C., & McGaugh, S. 1997, *PASP*, 109, 745, doi: [10.1086/133941](https://doi.org/10.1086/133941)
- Bothun, G. D., Impey, C. D., Malin, D. F., & Mould, J. R. 1987, *AJ*, 94, 23, doi: [10.1086/114443](https://doi.org/10.1086/114443)
- Bothun, G. D., Schombert, J. M., Impey, C. D., & Schneider, S. E. 1990, *ApJ*, 360, 427, doi: [10.1086/169133](https://doi.org/10.1086/169133)
- Brinchmann, J., Charlot, S., White, S. D. M., et al. 2004, *MNRAS*, 351, 1151, doi: [10.1111/j.1365-2966.2004.07881.x](https://doi.org/10.1111/j.1365-2966.2004.07881.x)
- Bruzual, G., & Charlot, S. 2003, *MNRAS*, 344, 1000, doi: [10.1046/j.1365-8711.2003.06897.x](https://doi.org/10.1046/j.1365-8711.2003.06897.x)
- Chabrier, G. 2003, *ApJL*, 586, L133, doi: [10.1086/374879](https://doi.org/10.1086/374879)
- Chilingarian, I. V., & Zolotukhin, I. Y. 2012, *MNRAS*, 419, 1727, doi: [10.1111/j.1365-2966.2011.19837.x](https://doi.org/10.1111/j.1365-2966.2011.19837.x)
- Cooke, K. C., Kartaltepe, J. S., Rose, C., et al. 2023, *ApJ*, 942, 49, doi: [10.3847/1538-4357/aca40f](https://doi.org/10.3847/1538-4357/aca40f)
- Daddi, E., Dickinson, M., Morrison, G., et al. 2007, *ApJ*, 670, 156, doi: [10.1086/521818](https://doi.org/10.1086/521818)
- Das, M., Boone, F., & Viallefond, F. 2010, *A&A*, 523, A63, doi: [10.1051/0004-6361/200913794](https://doi.org/10.1051/0004-6361/200913794)
- Das, M., O'Neil, K., Vogel, S. N., & McGaugh, S. 2006, *ApJ*, 651, 853, doi: [10.1086/507410](https://doi.org/10.1086/507410)
- de Blok, W. J. G., van der Hulst, J. M., & Bothun, G. D. 1995, *MNRAS*, 274, 235, doi: [10.1093/mnras/274.1.235](https://doi.org/10.1093/mnras/274.1.235)
- Dey, A., Schlegel, D. J., Lang, D., et al. 2019, *AJ*, 157, 168, doi: [10.3847/1538-3881/ab089d](https://doi.org/10.3847/1538-3881/ab089d)
- Di Teodoro, E. M., Posti, L., Ogle, P. M., Fall, S. M., & Jarrett, T. 2021, *MNRAS*, 507, 5820, doi: [10.1093/mnras/stab2549](https://doi.org/10.1093/mnras/stab2549)
- Du, W., Cheng, C., Wu, H., Zhu, M., & Wang, Y. 2019, *MNRAS*, 483, 1754, doi: [10.1093/mnras/sty2976](https://doi.org/10.1093/mnras/sty2976)
- Du, W., Wu, H., Lam, M. I., et al. 2015, *AJ*, 149, 199, doi: [10.1088/0004-6256/149/6/199](https://doi.org/10.1088/0004-6256/149/6/199)
- Elbaz, D., Daddi, E., Le Borgne, D., et al. 2007, *A&A*, 468, 33, doi: [10.1051/0004-6361:20077525](https://doi.org/10.1051/0004-6361:20077525)
- Galaz, G., Milovic, C., Suc, V., et al. 2015, *ApJL*, 815, L29, doi: [10.1088/2041-8205/815/2/L29](https://doi.org/10.1088/2041-8205/815/2/L29)
- Galaz, G., Frayer, D. T., Blańa, M., et al. 2022, *ApJL*, 940, L37, doi: [10.3847/2041-8213/aca146](https://doi.org/10.3847/2041-8213/aca146)
- Gunn, J. E., & Gott, J. Richard, I. 1972, *ApJ*, 176, 1, doi: [10.1086/151605](https://doi.org/10.1086/151605)
- Guo, K., Zheng, X. Z., Wang, T., & Fu, H. 2015, *ApJL*, 808, L49, doi: [10.1088/2041-8205/808/2/L49](https://doi.org/10.1088/2041-8205/808/2/L49)
- Hagen, L. M. Z., Seibert, M., Hagen, A., et al. 2016, *ApJ*, 826, 210, doi: [10.3847/0004-637X/826/2/210](https://doi.org/10.3847/0004-637X/826/2/210)
- Impey, C., & Bothun, G. 1989, *ApJ*, 341, 89, doi: [10.1086/167474](https://doi.org/10.1086/167474)
- Impey, C., & Bothun, G. 1997, *Annual Review of Astronomy and Astrophysics*, 35, 267, doi: [10.1146/annurev.astro.35.1.267](https://doi.org/10.1146/annurev.astro.35.1.267)
- Kasparova, A. V., Saburova, A. S., Katkov, I. Y., Chilingarian, I. V., & Bizyaev, D. V. 2014, *MNRAS*, 437, 3072, doi: [10.1093/mnras/stt1982](https://doi.org/10.1093/mnras/stt1982)
- Kent, S. M. 1985, *ApJS*, 59, 115, doi: [10.1086/191066](https://doi.org/10.1086/191066)
- Larson, R. B., Tinsley, B. M., & Caldwell, C. N. 1980, *ApJ*, 237, 692, doi: [10.1086/157917](https://doi.org/10.1086/157917)
- Lee, M.-Y., Stanimirović, S., Douglas, K. A., et al. 2012, *ApJ*, 748, 75, doi: [10.1088/0004-637X/748/2/75](https://doi.org/10.1088/0004-637X/748/2/75)
- Lelli, F., Fraternali, F., & Sancisi, R. 2010, *A&A*, 516, A11, doi: [10.1051/0004-6361/200913808](https://doi.org/10.1051/0004-6361/200913808)
- Licquia, T. C., & Newman, J. A. 2015, *ApJ*, 806, 96, doi: [10.1088/0004-637X/806/1/96](https://doi.org/10.1088/0004-637X/806/1/96)
- Matthews, L. D., Gao, Y., Uson, J. M., & Combes, F. 2005, *AJ*, 129, 1849, doi: [10.1086/428857](https://doi.org/10.1086/428857)
- Matthews, L. D., van Driel, W., & Monnier-Ragaigne, D. 2001, *A&A*, 365, 1, doi: [10.1051/0004-6361:20000002](https://doi.org/10.1051/0004-6361:20000002)
- McGaugh, S. S. 1994, *ApJ*, 426, 135, doi: [10.1086/174049](https://doi.org/10.1086/174049)
- McGaugh, S. S., & Bothun, G. D. 1994, *AJ*, 107, 530, doi: [10.1086/116874](https://doi.org/10.1086/116874)
- McGaugh, S. S., Schombert, J. M., & Bothun, G. D. 1995, *AJ*, 109, 2019, doi: [10.1086/117427](https://doi.org/10.1086/117427)
- McGaugh, S. S., Schombert, J. M., & Lelli, F. 2017, *ApJ*, 851, 22, doi: [10.3847/1538-4357/aa9790](https://doi.org/10.3847/1538-4357/aa9790)
- Mishra, A., Kantharia, N. G., Das, M., Omar, A., & Srivastava, D. C. 2017, *MNRAS*, 464, 2741, doi: [10.1093/mnras/stw2506](https://doi.org/10.1093/mnras/stw2506)
- Mishra, A., Kantharia, N. G., Das, M., Srivastava, D. C., & Vogel, S. N. 2015, *MNRAS*, 447, 3649, doi: [10.1093/mnras/stu2743](https://doi.org/10.1093/mnras/stu2743)
- Misiriotis, A., Xilouris, E. M., Papamastorakis, J., Boumis, P., & Goudis, C. D. 2006, *A&A*, 459, 113, doi: [10.1051/0004-6361:20054618](https://doi.org/10.1051/0004-6361:20054618)
- Moore, B., Katz, N., Lake, G., Dressler, A., & Oemler, A. 1996, *Nature*, 379, 613, doi: [10.1038/379613a0](https://doi.org/10.1038/379613a0)
- Morrissey, P., Conrow, T., Barlow, T. A., et al. 2007, *ApJS*, 173, 682, doi: [10.1086/520512](https://doi.org/10.1086/520512)
- Noeske, K. G., Faber, S. M., Weiner, B. J., et al. 2007a, *ApJL*, 660, L47, doi: [10.1086/517927](https://doi.org/10.1086/517927)

- Noeske, K. G., Weiner, B. J., Faber, S. M., et al. 2007b, *ApJL*, 660, L43, doi: [10.1086/517926](https://doi.org/10.1086/517926)
- Noll, S., Burgarella, D., Giovannoli, E., et al. 2009, *A&A*, 507, 1793, doi: [10.1051/0004-6361/200912497](https://doi.org/10.1051/0004-6361/200912497)
- Parkash, V., Brown, M. J. I., Jarrett, T. H., & Bonne, N. J. 2018, *ApJ*, 864, 40, doi: [10.3847/1538-4357/aad3b9](https://doi.org/10.3847/1538-4357/aad3b9)
- Pickering, T. E., Impey, C. D., van Gorkom, J. H., & Bothun, G. D. 1997, *AJ*, 114, 1858, doi: [10.1086/118611](https://doi.org/10.1086/118611)
- Pickering, T. E., van Gorkom, J. H., Impey, C. D., & Quillen, A. C. 1999, *AJ*, 118, 765, doi: [10.1086/300976](https://doi.org/10.1086/300976)
- Rahman, N., Howell, J. H., Helou, G., Mazzarella, J. M., & Buckalew, B. 2007, *ApJ*, 663, 908, doi: [10.1086/518554](https://doi.org/10.1086/518554)
- Saburova, A. S., Chilingarian, I. V., Kulier, A., et al. 2023, *MNRAS*, 520, L85, doi: [10.1093/mnrasl/slad005](https://doi.org/10.1093/mnrasl/slad005)
- Saintonge, A., Kauffmann, G., Wang, J., et al. 2011a, *MNRAS*, 415, 61, doi: [10.1111/j.1365-2966.2011.18823.x](https://doi.org/10.1111/j.1365-2966.2011.18823.x)
- Saintonge, A., Kauffmann, G., Kramer, C., et al. 2011b, *MNRAS*, 415, 32, doi: [10.1111/j.1365-2966.2011.18677.x](https://doi.org/10.1111/j.1365-2966.2011.18677.x)
- Saintonge, A., Tacconi, L. J., Fabello, S., et al. 2012, *ApJ*, 758, 73, doi: [10.1088/0004-637X/758/2/73](https://doi.org/10.1088/0004-637X/758/2/73)
- Saintonge, A., Catinella, B., Cortese, L., et al. 2016, *MNRAS*, 462, 1749, doi: [10.1093/mnras/stw1715](https://doi.org/10.1093/mnras/stw1715)
- Salim, S., Rich, R. M., Charlot, S., et al. 2007, *ApJS*, 173, 267, doi: [10.1086/519218](https://doi.org/10.1086/519218)
- Schlafly, E. F., & Finkbeiner, D. P. 2011, *ApJ*, 737, 103, doi: [10.1088/0004-637X/737/2/103](https://doi.org/10.1088/0004-637X/737/2/103)
- Schombert, J. 1998, *AJ*, 116, 1650, doi: [10.1086/300558](https://doi.org/10.1086/300558)
- Sprayberry, D., Impey, C. D., Bothun, G. D., & Irwin, M. J. 1995, *AJ*, 109, 558, doi: [10.1086/117300](https://doi.org/10.1086/117300)
- Sprayberry, D., Impey, C. D., Irwin, M. J., McMahon, R. G., & Bothun, G. D. 1993, *ApJ*, 417, 114, doi: [10.1086/173296](https://doi.org/10.1086/173296)
- Toomre, A. 1977, in *Evolution of Galaxies and Stellar Populations*, ed. B. M. Tinsley & D. C. Larson, Richard B. Gehret, 401
- Wuyts, S., Förster Schreiber, N. M., van der Wel, A., et al. 2011, *ApJ*, 742, 96, doi: [10.1088/0004-637X/742/2/96](https://doi.org/10.1088/0004-637X/742/2/96)